



Sedimentation waves on the Martian North Polar Cap: Analogy with megadunes in Antarctica



C. Herny^{a,*}, M. Massé^b, O. Bourgeois^a, S. Carpy^a, S. Le Mouélic^a, T. Appéré^{c,d},
I.B. Smith^e, A. Spiga^e, S. Rodriguez^d

^a Laboratoire de Planétologie et Géodynamique de Nantes, UMR 6112, CNRS, Université de Nantes, 2 chemin de la Houssinière, BP 92205, 44322 Nantes Cedex 3, France

^b Institut d'Astrophysique Spatiale, UMR 8617, CNRS, Université Paris 11, Bât. 121, 91405 Orsay, France

^c Institut de Planétologie et d'Astrophysique de Grenoble, UMR 5274, CNRS, Université Joseph Fourier, BP 53, F-38041 Grenoble Cedex 9, France

^d Laboratoire AIM, UMR 7158, CNRS, Université Paris 7, CEA-Saclay/DSM/IRFU/SAp, 91191 Gif-sur-Yvette Cedex, France

^e Laboratoire de Météorologie Dynamique, UMR 8539, CNRS, Université Pierre et Marie Curie, Paris, France

ARTICLE INFO

Article history:

Received 1 February 2014

Received in revised form 13 May 2014

Accepted 24 June 2014

Available online 10 July 2014

Editor: C. Sotin

Keywords:

ice sedimentation waves
megadunes
polar caps
Mars
Antarctica

ABSTRACT

Complex interactions between katabatic winds and the cryosphere may lead to the formation of sedimentation waves at the surface of ice sheets. These have been first described and named *snow megadunes* in Antarctica. Here we use topographic data, optical images, subsurface radar soundings and spectroscopic data acquired by Mars orbiters, to show that the surface of the Martian North Polar Cap displays two superimposed sets of sedimentation waves with differing wavelengths. These sedimentation waves have similarities with Antarctic snow megadunes regarding their surface morphology, texture, grain size asymmetry, and internal stratigraphic architecture. Both sets of Martian sedimentation waves present young ice and occasional sastrugi fields, indicative of net accumulation, on their shallow-dipping upwind sides, their tops and the intervening troughs. Old layers of dusty ice, indicative of net ablation, are exhumed on the steep-dipping downwind sides of the larger waves. Smooth surfaces of coarse-grained ice, indicative of reduced accumulation associated with sublimation metamorphism, cover the steep-dipping downwind sides of the smaller waves. These surface characteristics and the internal stratigraphy revealed by radar soundings are consistent with the interpretation that both sets of Martian sedimentation waves grow and migrate upwind in response to the development of periodic accumulation/ablation patterns controlled by katabatic winds. The recognition of these sedimentation waves provides the basis for the development of a common model of ice/wind interaction at the surface of Martian and terrestrial glaciers. Martian smaller waves, characterized by reduced net accumulation on their downwind sides, are analogous to Antarctic snow megadunes that have been described so far. A terrestrial equivalent remains to be discovered for the larger Martian waves, characterized by net ablation on their downwind sides.

© 2014 Elsevier B.V. All rights reserved.

1. Introduction

1.1. Scope of the paper

Ice accumulation and ablation patterns on glaciers are driven by complex mass and heat transfers between the atmosphere and the cryosphere. Winds, in particular, play a major role in the surface distribution of ice (Parish and Bromwich, 1991; Das et al., 2013) and may lead to the development of sedimentation waves, so-called megadunes, at the surface of ice sheets (Black and Budd, 1964; Fahnestock et al., 2000).

* Corresponding author.

The physical processes that govern the development of megadunes are still unclear because they have complex dynamics, which may involve ice redistribution by winds, ice metamorphism, and kinematic and thermal feedbacks between the ice sheet surface and the atmospheric boundary layer (Frezzotti et al., 2002a; Anschütz et al., 2006; Courville et al., 2007). The existence of megadunes has first-order effects on the glacial mass balance, the glacial flow and the characteristics of the atmospheric boundary layer; a clear understanding of their dynamics is therefore of primary importance for the climatic interpretation of ice records and for the assessment of processes and rates of mass and heat transfers in glaciers (Frezzotti et al., 2002a; Rémy and Frezzotti, 2006).

Snow megadunes have first been described in Antarctica. Here we show that sedimentation waves observed on the North Polar Cap of Mars (Cutts et al., 1979; Howard, 2000) have similarities with Antarctic snow megadunes in their morphology, internal stratigraphic architecture, surface texture, grain size, and in their dynamics. We illustrate these similarities with (1) topographic data from the Mars Orbiter Laser Altimeter (MOLA) digital elevation model (DEM) at 512 pixels/° resolution and 1 m vertical accuracy (Smith et al., 2001), (2) radar soundings from the SHARAD instrument (Seu et al., 2007), (3) optical images from the Context Camera (CTX) at up to 8 m/pixel resolution (Malin et al., 2007) and from the High Resolution Stereo Camera (HRSC) at up to 10 m/pixel resolution (Jaumann et al., 2007), and (4) hyper-spectral images from the Observatoire pour la Minéralogie, l'Eau, les Glaces et l'Activité (OMEGA) imaging spectrometer at 350 m to 4.8 km/pixel resolution (Bibring et al., 2004). The identification of these sedimentation waves brings new constraints on the physical processes that govern ice accumulation and ablation on Martian polar caps and may provide the basis for the development of a common model of ice/wind interaction at the surface of terrestrial and Martian glaciers.

1.2. Snow megadunes on Earth

Remotely-sensed optical and microwave data combined with field surveys have revealed the existence of extensive fields of megadunes on the Antarctic ice sheet (Black and Budd, 1964; Fahnestock et al., 2000; Frezzotti et al., 2002a, 2002b; Anshütz et al., 2006; Arcone et al., 2012). These megadunes develop preferentially where net ice accumulation rates are low (between 7 and 35 mm/yr w.e.; Frezzotti et al., 2002a) and under permanent and uniform katabatic wind regimes (Parish and Bromwich, 1991; Fahnestock et al., 2000; Albert et al., 2004; Lenaerts et al., 2012; Tomasi et al., 2012). Antarctic megadunes generally strike at high angles to katabatic wind streamlines. They are several tens of kilometers in length, about 2 to 5 km in wavelength, but only a few meters in amplitude. Their downwind sides are generally steeper (0.20°–0.30°) than their upwind sides (0.05°–0.25°) (Frezzotti et al., 2002a, 2002b). Their surface displays periodic ice distribution patterns (Goodwin, 1990; Frezzotti et al., 2002a; Albert et al., 2004). On the one hand, their upwind sides, their tops and the intervening troughs are generally covered by fields of fine-grained sastrugi, a few centimeters to 1.5 m in height and parallel to wind streamlines, indicative of enhanced accumulation. On the other hand, their downwind sides are generally characterized by smooth glazed surfaces underlain by thick layers of coarse-grained depth hoar formed by sublimation metamorphism, indicative of reduced net accumulation.

This asymmetry in surface ice properties and net accumulation rates across megadunes has been mapped from multispectral remote sensing data over wide areas of Antarctica (Fahnestock et al., 2000; Frezzotti et al., 2002a, 2002b; Scambos et al., 2007, 2012). It appears to be a long-term pattern according to radar stratigraphic soundings (Frezzotti et al., 2002a; Anshütz et al., 2006; Arcone et al., 2012). As net ice accumulation rates are larger on their upwind sides than on their downwind sides, snow megadunes behave as sedimentation waves that migrate upwind as they build up, which is at odds with the usual sense of migration of aeolian dunes (Bagnold, 1954).

1.3. The Martian North Polar Cap

The North Polar Cap is approximately 1300 km in diameter and its maximal thickness is about 3 km (Fig. 1) (Zuber et al., 1998). This cap is an accumulation of water ice layers with various amounts of dust (Grima et al., 2009). It rests on the remarkably flat northern plains of Mars (Fig. 1(b)) (Tanaka et al., 2008;

Putzig et al., 2009). Its surface is subject to a permanent and nearly uniform regime of katabatic winds that turn westward under the effect of the Coriolis force as they descend and accelerate from the polar high towards the ice cap margin (Fig. 1(a)) (Howard, 2000; Spiga, 2011; Massé et al., 2012). The pressure is low (6.5–9.5 mbar Haberle et al., 2008) and the surface temperature of the North Polar Cap varies from 145 K in winter ($270^\circ < L_s < 360^\circ$) to 220 K in summer ($90^\circ < L_s < 180^\circ$) (Jakosky and Farmer, 1982; Forget and Pollak, 1996; Pankine et al., 2010).

Ice accumulation processes on the North Polar Cap may include precipitation of ice crystals from the atmosphere (Whiteway et al., 2009) and direct condensation of water vapor onto the ice cap surface (Ivanov and Muhleman, 2000). Ablation occurs dominantly by sublimation during the north polar summer due to the low partial pressure of water vapor in the atmosphere ($<10^{-2}$ mbar) and the seasonal increase in temperature (Jakosky and Farmer, 1982; Ivanov and Muhleman, 2000; Pankine et al., 2010). Long-term net ice accumulation rates, as computed from tuning the stratigraphy of the upper ~500 m of the North Polar Cap with Martian orbital cycles, are close to 0.5 mm/yr (Laskar et al., 2002; Fishbaugh and Hvidberg, 2006; Milkovich et al., 2008), whereas short-term rates derived from the obliteration of recent impact craters are an order of magnitude higher (Herkenhoff and Plaut, 2000; Banks et al., 2010). This discrepancy might reveal either a recent increase in the net ice accumulation rate or a difference between short-term and long-term accumulation rates. Whatever its reason, this supports the idea that the relationship between the ice cap stratigraphy and the chronology of past orbital cycles is not trivial (Sori et al., 2014).

2. Two sets of sedimentation waves on the Martian North Polar Cap

2.1. Large sedimentation waves

The surface morphology of the North Polar Cap is dominated by large spiral-shaped topographic waves that strike at high angles to katabatic winds (Fig. 1) (Howard, 2000; Massé et al., 2012; Smith et al., 2013). These topographic waves define alternating ridges and troughs, hundreds of kilometers in length, 60 km in average wavelength and hundreds of meters in amplitude. The downwind sides of the ridges are steeper (2° – 15°) than their upwind sides (0.5° – 7°) (Howard, 2000; Pathare and Paige, 2005). The surface composition differs between both sides (Fig. 2): nearly pure and young ice uniformly covers their upwind sides and tops, while old layers of ice mixed with dust and hydrated minerals are exhumed on their downwind sides (Howard et al., 1982; Massé et al., 2010, 2012).

These large topographic waves correspond to sedimentation waves that migrate upwind as they build up, in response to an asymmetry in the accumulation/ablation pattern (Fig. 1(b), Fig. 2(b) and (c)) (Smith and Holt, 2010; Smith et al., 2013). Stratigraphic unconformities visible on SHARAD radargrams and differences in ice surface properties reveal that long-term net accumulation occurs on their upwind sides and tops, while long-term net ablation, leading to exhumation of old ice and dust layers, occurs on their downwind sides (Fig. 1(b), Fig. 2(a) and (c)) (Cutts et al., 1979; Squyres, 1979; Howard, 2000; Ivanov and Muhleman, 2000; Ng and Zuber, 2006; Smith and Holt, 2010; Massé et al., 2010, 2012; Smith et al., 2013). This asymmetry in the accumulation/ablation pattern has been attributed to the combined action of (1) katabatic winds and (2) sublimation/condensation processes due to the volatile nature of water ice at Martian conditions of pressure and temperature (Howard, 2000; Ivanov and Muhleman, 2000; Ng and Zuber, 2006; Smith and Holt, 2010; Massé et al., 2012).

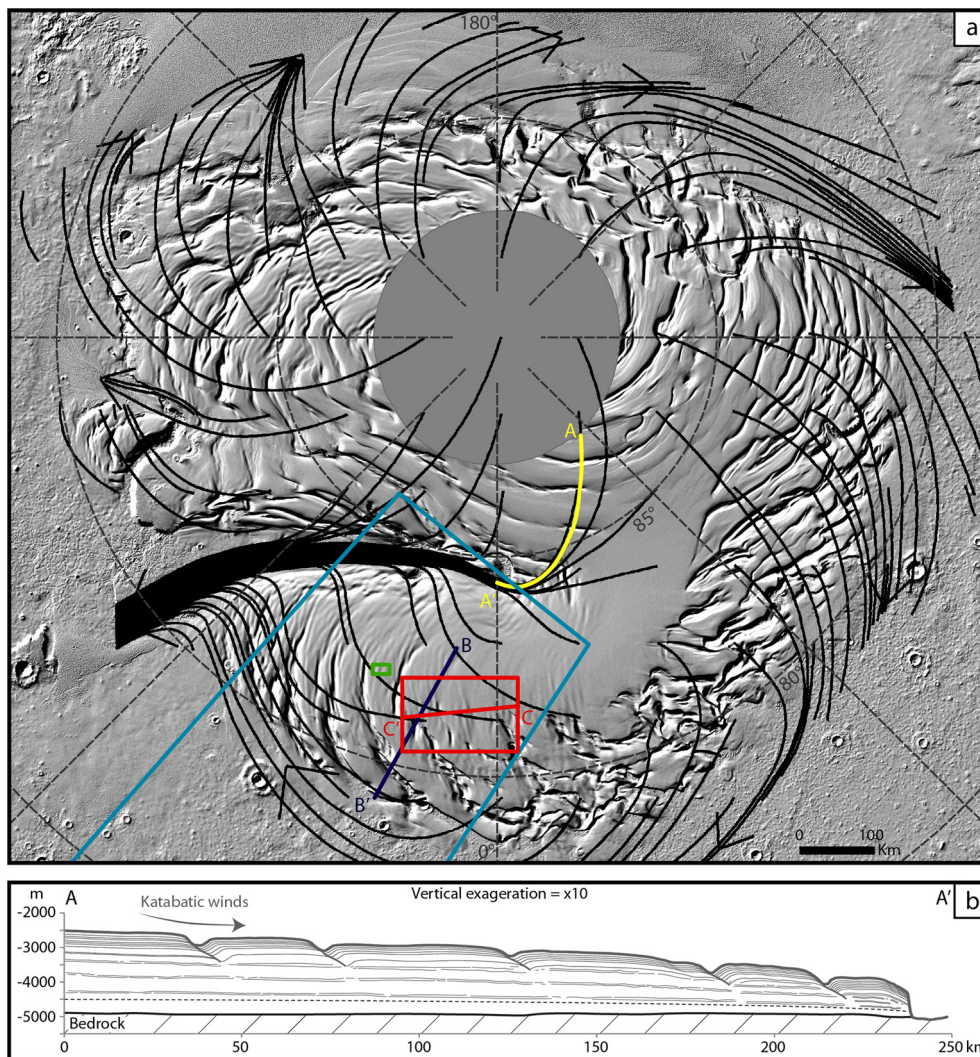


Fig. 1. (a) Shaded-relief map of the North Polar Cap of Mars computed from the MOLA DEM (Zuber et al., 1998), with superimposed katabatic wind streamlines from Massé et al. (2012). Profile AA' corresponds to the location of the transect presented in (b). Profile BB' corresponds to the location of Fig. 2. The study area (red box) is located on a small sedimentation wave field of the Gemina Lingula lobe. Profile CC' corresponds to the topographic profile location of Fig. 3 and Fig. 6. The blue box corresponds to the footprint of OMEGA hyperspectral cube ORB1090_1. The green box corresponds to the footprint of Fig. 7. (b) Interpretative cross-section along profile AA' (delineated by yellow line in (a)), based on ice surface topographic profile (thick gray line) derived from the MOLA DEM and radar reflectors. (For interpretation of the references to color in this figure legend, the reader is referred to the web version of this article.)

As noted by Smith et al. (2013), the overall morphology and stratigraphy of these large sedimentation waves are comparable to those of Antarctic megadunes, though they differ by one order of magnitude in wavelength and by two orders of magnitude in amplitude. Another difference is that their downwind sides are subject to net ablation (Howard, 2000; Cutts et al., 1979; Ng and Zuber, 2006; Smith and Holt, 2010; Massé et al., 2010, 2012; Smith et al., 2013), whereas megadune downwind sides in Antarctica are most commonly subject to reduced net accumulation (Frezzotti et al., 2002a; Albert et al., 2004; Anshütz et al., 2006; Courville et al., 2007).

2.2. Small sedimentation waves

Smaller linear topographic waves, also called undulations, are superimposed on the upwind sides of the large spiral-shaped topographic waves of the North Polar Cap (Fig. 2) (Cutts et al., 1979; Howard, 2000; Smith et al., 2013). These are particularly visible on the Gemina Lingula lobe (Fig. 1(a)). Various origins have been proposed for these small topographic waves, including (1) periodic advance and retreat of the polar cap (Cutts et al., 1979), (2) poleward

migration of spiral-shaped troughs (Squyres, 1979), (3) closure of ancient spiral-shaped troughs by viscous relaxation (Pathare and Paige, 2005), (4) filling of ancient spiral-shaped troughs (Rodríguez et al., 2007) and (5) interactions between atmospheric waves and the ice cap (Howard, 2000; Smith et al., 2013).

The small topographic waves have morphological, textural and stratigraphic similarities with Antarctic megadunes. (1) They are organized in periodic sub-parallel patterns that strike at high angles to katabatic wind streamlines. (2) Their downwind sides are generally steeper (0.2° – 2°) than their upwind sides (0.02° – 1°) (Fig. 3). (3) They are hundreds of kilometers in length, about 10 km in wavelength and 10 to 50 m in amplitude (Cutts et al., 1979). Though they are about 2 to 5 times as large as Antarctic megadunes, their amplitude/wavelength ratio is on the same order of magnitude of about 1/1000. (4) SHARAD radar soundings reveal that their internal stratigraphy undulates conformably with their surface topography (Fig. 2). This indicates that the small topographic waves are the surface expression of internal sedimentation waves. No stratigraphic unconformity is however visible on available SHARAD radargrams on the Gemina Lingula lobe, which suggests that both sides of these sedimentation waves are

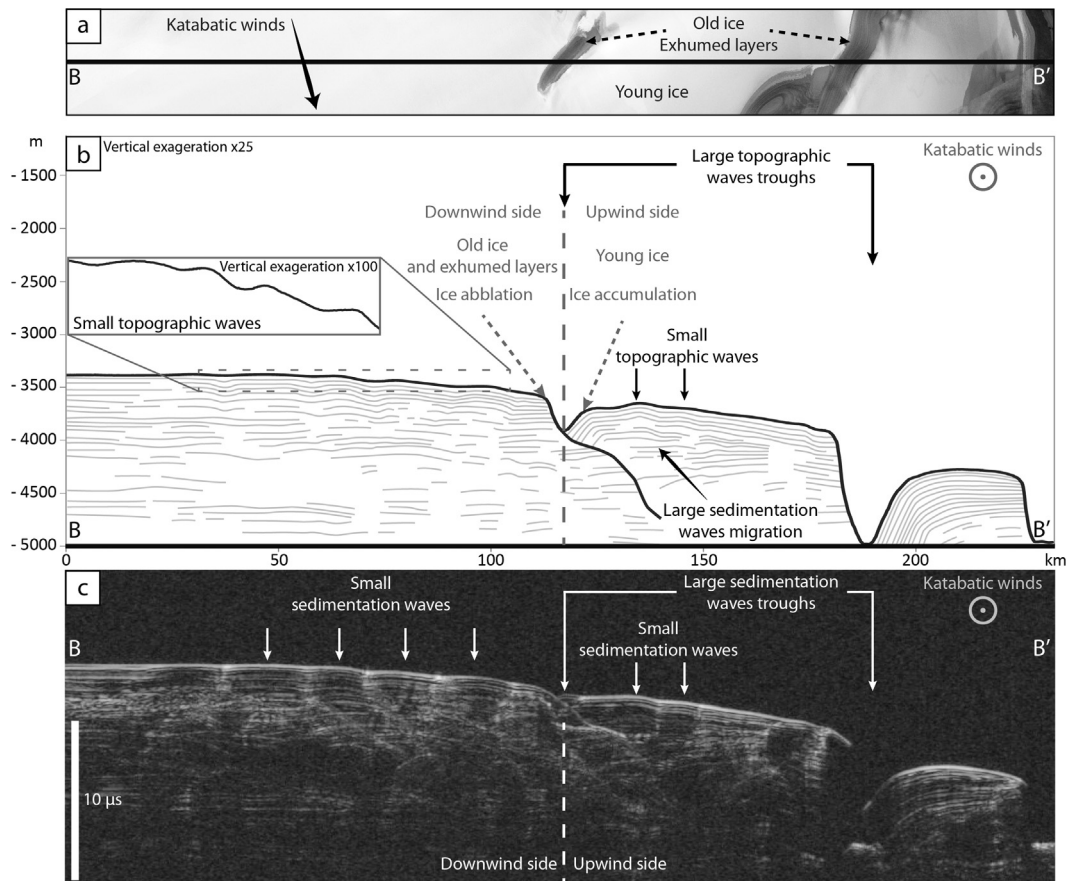


Fig. 2. (a) Mosaic of HRSC images ($L_s = 134.9^\circ$ to 137.9°) showing the surface of the ice cap along profile BB' (Fig. 1). Dusty ice layers are exposed on the downwind side of the large topographic waves, while pure ice covers their upwind sides and tops. (b) Interpretative cross-section along profile BB' (delineated by dark blue line in (a) and in Fig. 1), based on ice surface topographic profile (thick black line) derived from the MOLA DEM and radar reflectors (thin grey lines) visible in (c). (c) Portion of SHARAD radargram 4428_01 along the profile BB'. Unfortunately, no SHARAD radargram parallel to wind streamlines is available on the Gemina Lingula lobe; though this radargram strikes at high angle to the wind azimuth, the internal stratigraphic architecture of large and small topographic waves is visible and correspond to sedimentation waves.

subject to long-term net accumulation. The high angle orientation of the radar profile (Fig. 2(c)) to the wind streamlines do not allow us to conclude to a migration direction of the small sedimentation waves. (5) Optical CTX images, acquired during the Martian north polar summer to avoid disturbances due to winter condensation of CO_2 and H_2O ices (Appéré et al., 2011), reveal that the surface texture of the North Polar Cap comprises alternating smooth and rough stripes. These are parallel to and correlated with the small sedimentation waves (Fig. 4). The smooth stripes do not display a specific texture at the CTX image resolution, while the rough stripes are characterized by longitudinal ridges and furrows, several kilometers in length and between 100 and 500 m apart. The ridges and furrows are parallel to wind streamlines and resemble “severe sastrugi”, up to 1.5 m in height, observed at the surface of some Antarctic megadune fields (Frezzotti et al., 2002a, 2002b). The rough stripes occur preferentially on the sedimentation wave upwind sides, crests and intervening troughs, while the smooth stripes occur dominantly on their downwind sides. This periodically striped surface texture is similar to that of Antarctic megadune fields, where sastrugi fields alternate with smooth glazed surfaces (Frezzotti et al., 2002a; Albert et al., 2004).

3. Variations in ice optical grain size on the Martian North Polar Cap

In Antarctica, the asymmetry of ice grain size across megadunes affects the optical reflectance spectrum of the ice surface, thus providing a way to map megadunes from multispectral optical images

(Fahnestock et al., 2000; Frezzotti et al., 2002a, 2002b; Scambos et al., 2007, 2012). Here we investigate similar spectroscopic variations over the Gemina Lingula lobe with hyperspectral data acquired by the OMEGA imaging spectrometer.

3.1. Depth of water ice absorption bands

Water ice displays specific spectroscopic absorption bands at optical wavelengths. The depth of these absorption bands depends on the physical properties of the ice (including grain size, crystal shape and impurity content) (Warren, 1982; Clark and Roush, 1984; Lucey and Clark, 1985). The surface properties of the Martian North Polar Cap can therefore be investigated by monitoring water ice absorption band depths in data acquired by the OMEGA imaging spectrometer.

For each pixel of an image, OMEGA acquires a spectrum of the surface in 352 narrow spectral channels. It includes one detector in the Visible–Near InfraRed, between 0.36 and $1.07 \mu\text{m}$, and another one in the Short Wavelength InfraRed, between 0.93 and $5.1 \mu\text{m}$ (Bibring et al., 2004). We selected data acquired during the Martian northern summer to minimize the effects of the seasonal CO_2 and H_2O frost coverage (Appéré et al., 2011). The atmospheric spectral contribution was removed using the empirical atmospheric transmission law defined by Langevin et al. (2005).

Hyperspectral cube ORB1090_1, acquired at $L_s = 119.2^\circ$, covers the Gemina Lingula lobe with a pixel size of 2.5 km, smaller than the wavelength of the small sedimentation waves (Fig. 3). Spectral signatures observed on these sedimentation waves are typical of pure water ice, with higher reflectance values in the visible than

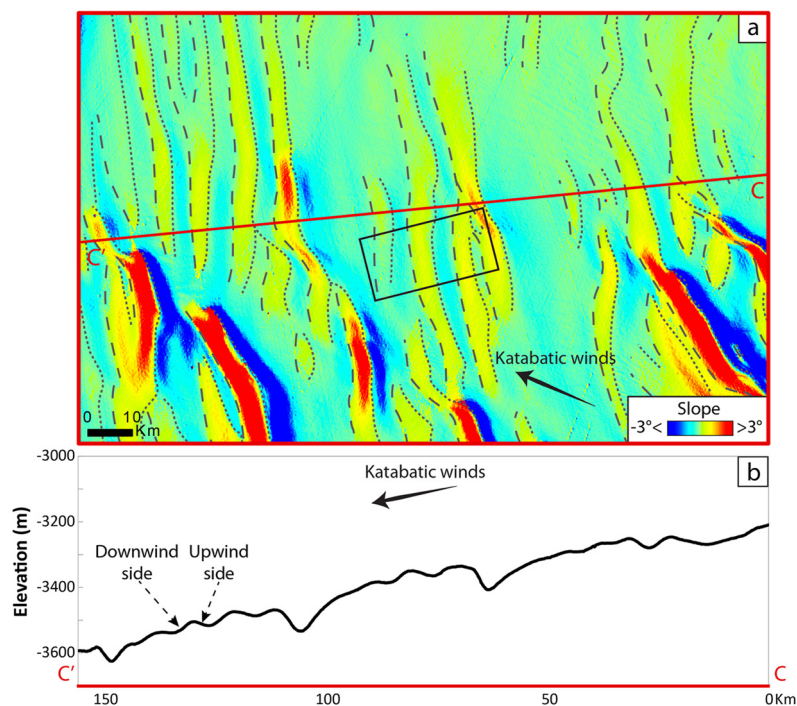


Fig. 3. (a) Slope map derived from the MOLA DEM over the area outlined by a red box in Fig. 1, emphasizing small sedimentation waves on the Gemina Lingula lobe. The black dotted and dashed lines represent topographic troughs and crests respectively. Negative slope values (green to blue) correspond to sedimentation wave downwind sides and positive slope values (yellow to red) to their upwind sides. Small wavelength sedimentation waves have slopes values comprised between -2° and $+2^\circ$ and are generally steeper on their downwind sides (b). The steepest positive and negative slopes in the image ($< -3^\circ$ or $> +3^\circ$) correspond to the tips of large sedimentation waves. (b) Ice surface elevation along profile CC' delineated by red line in (a). (For interpretation of the references to color in this figure legend, the reader is referred to the web version of this article.)

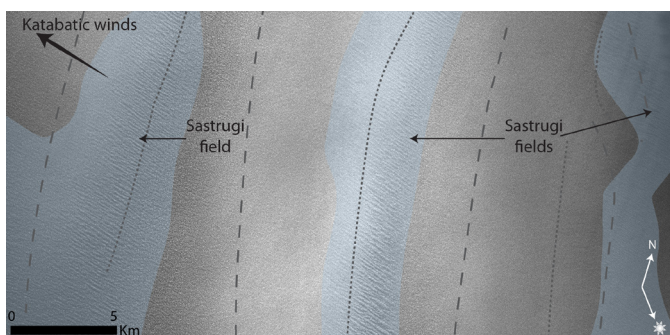


Fig. 4. Portion of CTX image P20_008995_2593_XL_79N001W, acquired at $L_s = 90.96^\circ$ and outlined by black box in Fig. 3(a), showing fields of wind-parallel sastrugi (highlighted in light blue) alternating with sastrugi-free fields on the small wavelength sedimentation waves. (For interpretation of the references to color in this figure legend, the reader is referred to the web version of this article.)

in the infrared and four large absorption bands at 1.04, 1.25, 1.50 and 2.02 μm (Fig. 5). Reflectance values in the visible are generally similar on both sides of the small sedimentation waves, but water ice absorption bands in the near infrared are generally deeper on their downwind sides than on their upwind sides.

To emphasize these spectral variations, we mapped the depth of the 1.25 μm absorption band over the Gemina Lingula lobe. We selected this band because the 1.50 and 2.02 μm bands become saturated with increasing grain size (Brown and Calvin, 2012) and because computing the 1.04 μm band depth is impeded by the change of OMEGA detector between 0.93 and 1.07 μm (Fig. 5). The 1.25 μm absorption band depth, BD (1.25 μm), is computed as follows:

$$BD(1.25 \mu\text{m}) = 1 - \frac{R(1.25)}{(0.5 \times R(1.36) + 0.5 \times R(1.16))} \quad (1)$$

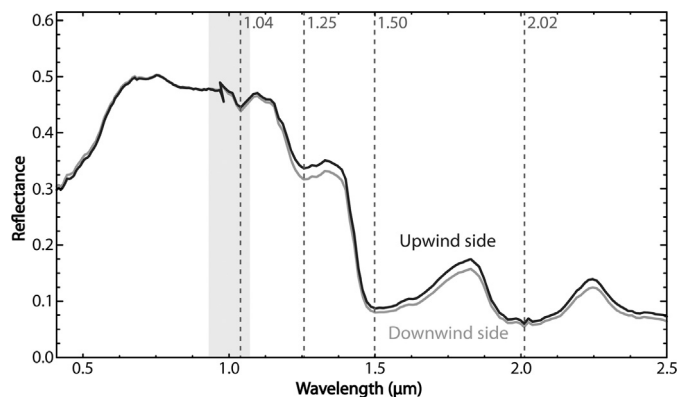


Fig. 5. Reflectance spectra of small sedimentation wave upwind sides (black line) and downwind sides (grey line). Black and grey spectra correspond to the average of several spectra of OMEGA cube ORB1090_1 acquired respectively on the upwind sides (black dotted lines in Fig. 6(b)) and on the downwind sides (grey dotted lines in Fig. 6(b)). Vertical dashed lines indicate wavelengths of diagnostic water ice absorption bands. The grey area corresponds to the change of OMEGA detector between 0.93 and 1.07 μm .

where $R(x)$ is the reflectance value at the $x \mu\text{m}$ wavelength. In order to reduce the spectral noise, the reflectance value at a given wavelength is taken as the median of the reflectance values measured in three adjacent spectral channels centered on this wavelength (Massé et al., 2010, 2012).

The resulting map reveals linear stripes of alternatively deeper and shallower water ice absorption band at 1.25 μm (Fig. 6(a) and (b)). These periodic spectroscopic variations are correlated with the small sedimentation waves. Absorption maxima are observed on their downwind sides whereas absorption minima are observed on their upwind sides (Fig. 6(c)). This result, obtained on Mars from hyperspectral data, is comparable to spectroscopic variations observed on Antarctic megadunes from multispectral

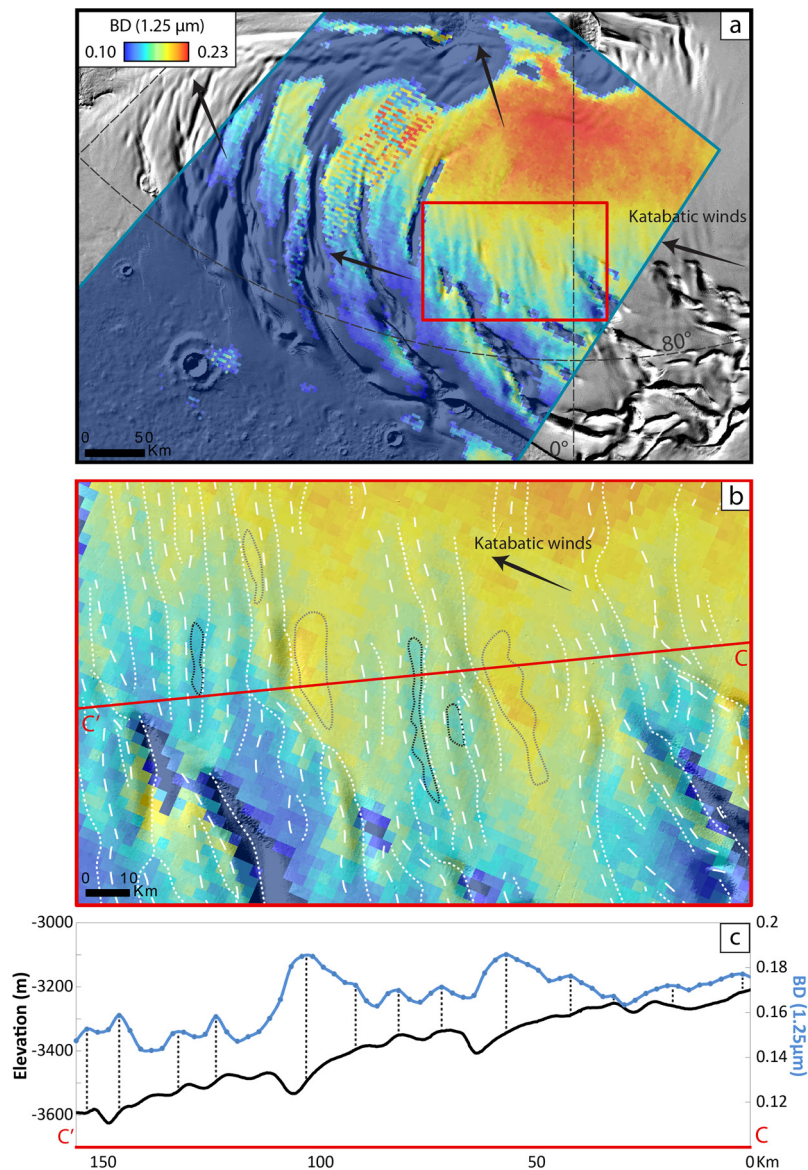


Fig. 6. (a) Map of ice absorption band depth at 1.25 μm , derived from hyperspectral OMEGA cube ORB1090_1, acquired at $L_s = 119.2^\circ$ during Martian Year 27 (cube footprint delineated by a blue box), overlaid on a shaded-relief map of the Gemina Lingula lobe computed from MOLA DEM. The map reveals linear stripes of alternatively shallower (blue) and deeper (orange) absorption at 1.25 μm . (b) Zoom on the area outlined by a red box in (a). The white dotted and dashed lines represent sedimentation wave troughs and crests respectively. The grey and black dotted contours refer to the footprint of the regions of interest used to compute average spectra on the sedimentation wave downwind and upwind sides respectively. (c) Ice surface elevation (black line) compared to band depth at 1.25 μm (blue line) along profile CC' delineated by red line in (b). (For interpretation of the references to color in this figure legend, the reader is referred to the web version of this article.)

data (Fahnestock et al., 2000; Frezzotti et al., 2002a, 2002b; Scambos et al., 2007, 2012).

3.2. Interpretation

The correlation between spectroscopic variations and small sedimentation waves on the North Polar Cap can be caused by two parameters: these are the viewing geometry of the OMEGA observation (incidence and emergence angles of light on the surface) and the ice surface properties (including impurity content, grain size and crystal shape) (Warren, 1982; Clark and Roush, 1984; Lucey and Clark, 1985). The effects of these parameters on the observed spectroscopic variations are now discussed.

Changes in surface topographic slopes produce changes in the incidence and emergence angles of the light recorded by orbital imaging spectrometers. Photometric effects associated with these changes in the viewing geometry alter the shape of the spectral

continuum and the absolute value of the reflectance (Nolin, 1998; Nolin and Dozier, 2000; Vincendon et al., 2007; Dumont et al., 2010). However, absorption band depths computed as in Eq. (1) are theoretically insensitive to the shape of the continuum and thereby to topographic slopes (Clark and Roush, 1984; Nolin and Dozier, 2000; Frezzotti et al., 2002a, 2002b; Painter et al., 2003). In order to rule out definitively these effects as possible causes for the observed correlation between spectroscopic variations at 1.25 μm and the small sedimentation waves, we analyzed several OMEGA cubes acquired with various viewing geometries (Fig. 7). The band depth variations at 1.25 μm occur at the same locations on the small sedimentation waves (Fig. 7(a) and (c)), though the illumination directions differ greatly between the cubes (Fig. 7(b) and (d)). For all the analyzed cubes, maximal absorptions occur on sedimentation wave downwind sides, while minimal absorptions occur on their upwind sides. By contrast, the variations of the 1.25 μm absorption band depth is independent of the incidence

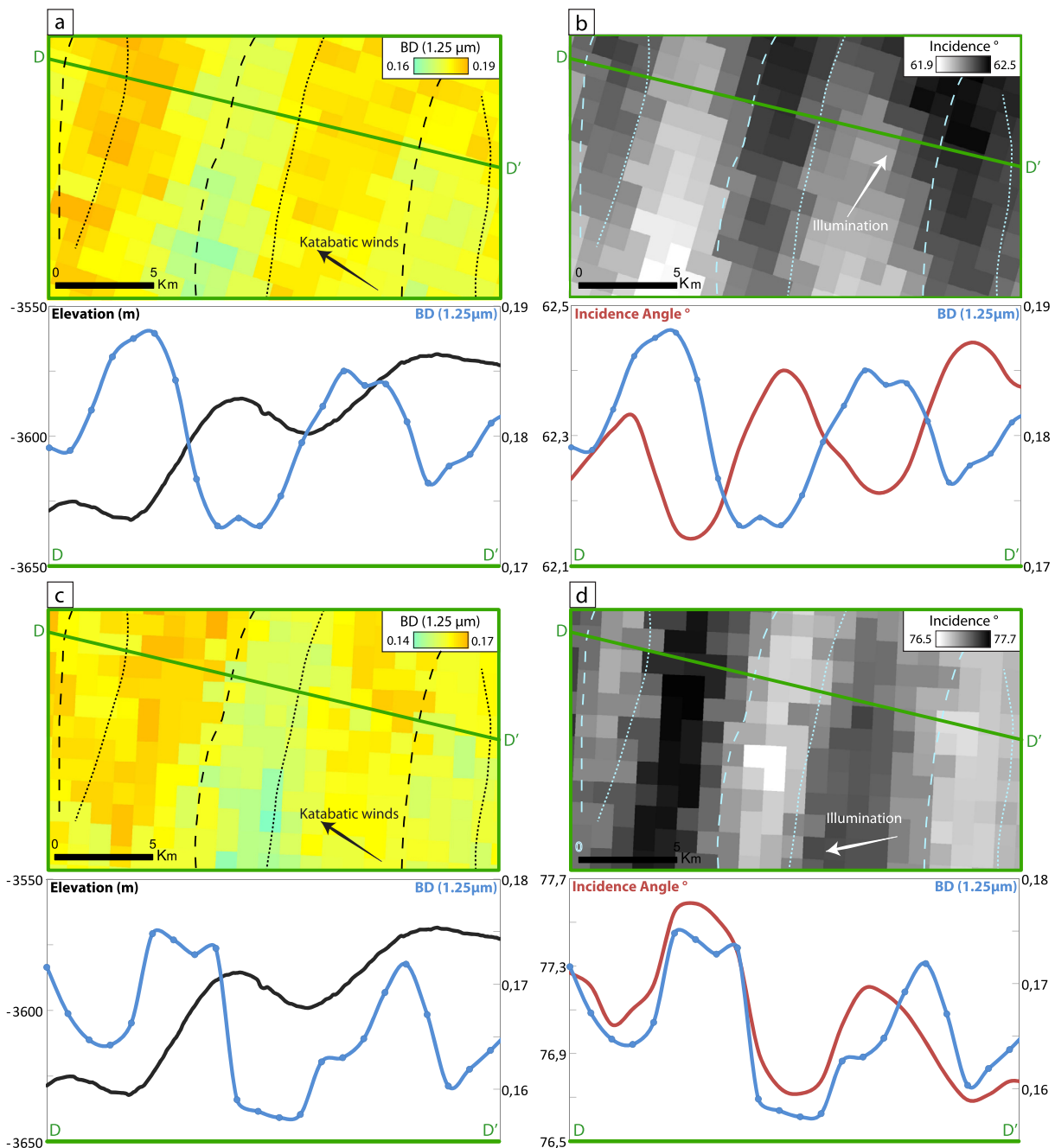


Fig. 7. Comparison of the 1.25 μm absorption band depth derived from two OMEGA cubes with differing viewing geometries acquired on a subset of the Gemina Lingula lobe outlined by green box in Fig. 1. The dotted and dashed lines represent sedimentation wave troughs and crests respectively. Elevation and band depth along profile DD' are represented below each map. (a) and (c) Maps of 1.25 μm absorption band depth derived from hyperspectral OMEGA cubes ORB1150_2 ($L_s = 127.1^\circ$) and ORB1200_0 ($L_s = 133.5^\circ$) respectively. Profiles DD' show ice surface elevation derived from the MOLA DEM (black lines) compared to 1.25 μm band depth (blue lines). (b) and (d) Maps of local incidence angles associated to hyperspectral OMEGA cubes ORB1150_2 and ORB1200_0. The illumination orientations (white arrows) are opposite between these two observations. Profiles DD' show local incidence angles (red lines) compared to 1.25 μm band depth (blue lines). (For interpretation of the references to color in this figure legend, the reader is referred to the web version of this article.)

angle (Fig. 7(b) and (d)): both vary in phase for one observation geometry (Fig. 7(d)) while band depth is in antiphase for an opposite illumination direction (Fig. 7(b)). This observation, together with the very small range of incidence variations (0.4° in (b) and 1.2° in (d)), lead us to the conclusion that photometric effects due to topographic slopes do not cause these spectroscopic variations.

The North Polar Ice Cap is contaminated by mafic dust and hydrated minerals, particularly on the large sedimentation wave downwind sides (Massé et al., 2010, 2012). The presence of impurities in ice tends to flatten its reflectance spectrum and may introduce mineral hydration absorption bands that can interfere

with water ice absorption bands (Lucy and Clark, 1985; Massé et al., 2010). Experimental measurements and modeling studies on water ice and dust mixtures reveal that small amounts of dust produce a strong decrease of reflectance in the visible part of the spectrum while they do not affect significantly the reflectance of ice in the near-infrared (Warren, 1982; Lucy and Clark, 1985). By contrast, the reflectance in the visible does not vary significantly across the small sedimentation waves of the North Polar Cap (Fig. 5). The diagnostic absorption bands of polar dust (Massé et al., 2010, 2012) are not detected on the small sedimentation waves in our study area. These observations indicate that the dust

content of the ice is both constant and low. Therefore, it cannot be responsible for the observed spectroscopic variations over the small topographic waves.

Spatial variations in accumulation/ablation rates and in post-depositional metamorphism intensity lead to spatial variations in the shape and size of ice crystals at the surface of glaciers. This has been well documented in Antarctica, where fine-grained pristine ice generally covers areas of enhanced net accumulation, while coarse-grained metamorphosed ice is generally exposed in areas of reduced net accumulation (Goodwin, 1990; Frezzotti et al., 2002a; Gay et al., 2002; Albert et al., 2004; Courville et al., 2007). These variations may in turn affect the spectroscopic signature of the ice surface on remotely-sensed images (Fahnestock et al., 2000; Frezzotti et al., 2002a, 2002b; Langevin et al., 2005; Courville et al., 2007; Scambos et al., 2007, 2012). The optical grain size refers to the mean free path of photons in the ice pack between two scattering events and it depends on the ice composition, crystals size and shape (Warren, 1982; Lucey and Clark, 1985; Scambos et al., 2007). Experimental and modeling studies reveal that infrared reflectance values generally decrease and water ice absorption band depths generally increase as the optical grain size increases (Warren, 1982; Lucey and Clark, 1985; Nolin and Dozier, 2000; Langevin et al., 2005; Brown and Calvin, 2012; Taffin et al., 2012). On this basis, it is reasonable to assume that the spectroscopic variations observed across the small sedimentation waves of the Martian North Polar Cap are due to smaller optical grain sizes on their upwind sides than on their downwind sides. By analogy with Antarctica, this difference may be attributed to an asymmetry in surface ice distribution processes on the small sedimentation waves: smaller grains on their upwind sides would correspond to pristine ice indicative of enhanced net accumulation, while coarser grains on their downwind sides would correspond to metamorphosed ice indicative of reduced net accumulation.

4. Discussion

4.1. Analogy between Martian sedimentation waves and Antarctic megadunes

Sedimentation waves on the Martian North Polar Cap are similar to Antarctic megadunes in many respects, although they differ in amplitude and wavelength.

(1) They are organized in periodic sub-parallel patterns that strike at high angles to katabatic wind streamlines.

(2) Their downwind sides are generally steeper than their upwind sides.

(3) They are associated to periodic variations in the properties of the ice surface. The large sedimentation waves are covered by pure young ice on their upwind sides and tops, while layers of dusty old ice are exhumed on their downwind sides. The small sedimentation waves are generally covered by rough surfaces resembling terrestrial sastrugi fields on their upwind sides, their crests and the intervening troughs, while smooth areas are exposed on their downwind sides.

(4) Spectroscopic variations at the surface of the small sedimentation waves are consistent with the presence of fine-grained pristine ice indicative of enhanced net accumulation on their upwind sides and of coarser-grained metamorphosed ice, indicative of reduced net accumulation on their downwind sides. We were not able to detect equivalent variations in ice grain size on the large sedimentation waves, because exhumed dust alters the ice spectrum on their downwind sides (Massé et al., 2010, 2012). Nonetheless, old ice layers exposed by sublimation on these large sedimentation wave downwind sides (Massé et al., 2010, 2012; Smith and Holt, 2010) are expected to be composed of coarse-grained metamorphosed ice.

(5) Radar stratigraphic soundings reveal an asymmetry in long-term ice distribution patterns across the large sedimentation waves: net accumulation occurs on their upwind sides and tops, while net ablation occurs on their downwind sides (Smith and Holt, 2010). A similar stratigraphic asymmetry cannot be detected unambiguously for the small sedimentation waves on the study area; the available SHARAD radargrams however show that their internal stratigraphy is conformable with their undulating surface topography and that both sides are subject to net accumulation.

4.2. Toward a common model of ice/wind interaction on Earth and Mars

The development of Antarctic megadunes has been attributed to dynamic feedbacks between the atmosphere and the cryosphere (Fuji and Kusunoki, 1982; Frezzotti et al., 2002a; Albert et al., 2004; Courville et al., 2007; Scambos et al., 2012; Dacic et al., 2013). The acceleration of katabatic winds on their downwind sides enhances ablation, thus reducing long-term net accumulation and leading to prolonged sublimation metamorphism that drives the formation of coarse-grained ice and glazed surfaces. By contrast, fine-grained ice accumulates on their upwind sides, and deceleration of katabatic winds above these sastrugi-covered surfaces further enhances accumulation. Over time, the accumulated ice progressively buries uphill glazed surfaces and the megadunes migrate upwind.

We propose that dynamics comparable to those of Antarctic megadunes are involved in the development of large and small sedimentation waves on the Martian North Polar Cap. Our favored model is illustrated in Fig. 8. Fine-grained pristine ice accumulates at the surface of the ice cap by condensation of water vapor transported by katabatic winds, and/or by deposition of wind-blown crystals formed in the atmosphere (Whiteway et al., 2009; Smith et al., 2013). Katabatic winds partially depleted from their water vapor content flow over sedimentation wave downwind side, thus enhancing sublimation there and generating either long-term net ablation or reduced long-term net accumulation. Enhanced sublimation leads to the formation of coarse-grained metamorphosed ice on the sedimentation wave downwind side and the water vapor produced by sublimation is transported by katabatic winds toward the next sedimentation wave upwind side. There, the physical conditions are favorable for the water ice to condense back to the ice cap surface, thus enhancing long-term net accumulation. This model is consistent with previous inferences that sublimation, condensation, katabatic winds and atmospheric waves are involved in the development of sedimentation waves on Martian polar caps (Howard, 2000; Ivanov and Muhleman, 2000; Smith and Holt, 2010; Massé et al., 2012; Smith et al., 2013).

Martian topographic waves are larger in wavelength and amplitude than Antarctic megadunes. This difference reflects differences in gravity, atmospheric conditions (e.g., pressure, temperature, density, viscosity, atmospheric boundary layer) and ice properties (e.g., crystal sizes and shapes, density, porosity, presence of dust) between the two planets (Claudin and Andreotti, 2006; Andreotti et al., 2009; Bourke et al., 2010). Megadunes in Antarctica and sedimentation waves on Mars thus provide two natural cases with different boundary conditions, against which models of ice/wind interactions at the surface of glaciers may be tested. As suggested by Frezzotti et al. (2002a), Dacic et al. (2013) and Smith et al. (2013), the Froude number controls these interactions as it does for sedimentation waves, antidunes and cyclic steps in sub-aerial and submarine environments (Flood, 1988; Lee et al., 2002; Kostic et al., 2010).

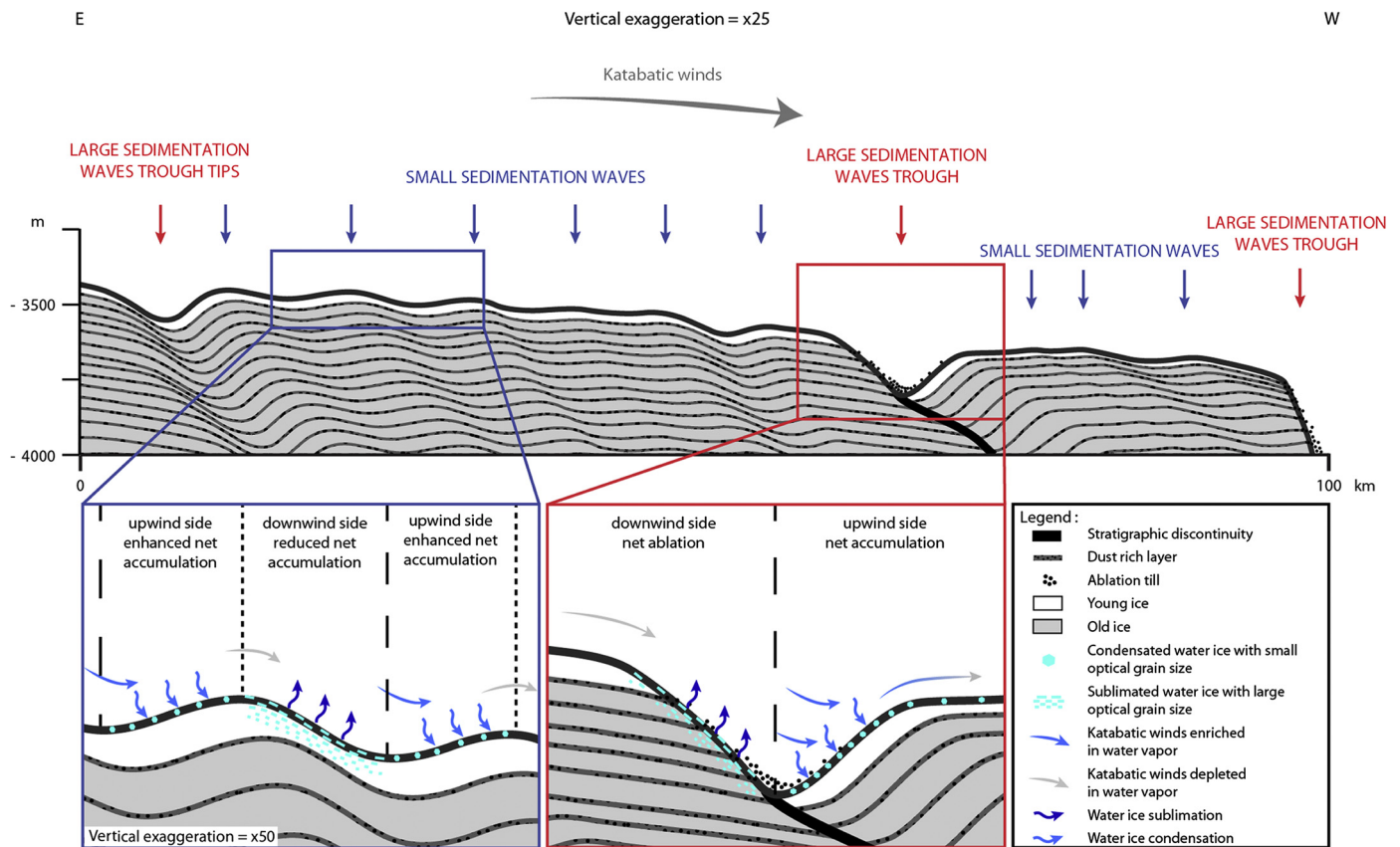


Fig. 8. Interpretative cross-section of Gemina Lingula, illustrating the surface topography, the internal architecture and the physical processes involved in the dynamics of the two sets of Martian ice sedimentation waves.

4.3. Difference between large and small sedimentation waves

The relative magnitude of ice distribution processes differs between large and small sedimentation waves (Fig. 8). The internal stratigraphic architecture and the surface spectroscopic properties of the small ones are consistent with enhanced net accumulation on their upwind sides and reduced net accumulation on their downwind sides. By contrast, the large ones are subject to net accumulation on their upwind sides and net ablation on their downwind sides (Howard, 1978, 2000; Howard et al., 1982; Cutts et al., 1979; Ng and Zuber, 2006; Smith and Holt, 2010; Massé et al., 2010, 2012; Smith et al., 2013). The analogy with Antarctic megadunes is therefore probably more relevant for the small Martian sedimentation waves than for the large ones.

This difference also suggests that, although the large and small Martian sedimentation waves are comparable in their overall dynamics, additional mechanisms must dramatically promote ablation on the downwind sides of the large ones. These mechanisms most probably involve enhanced friction and sublimation due to strong wind acceleration associated to the formation of katabatic jumps in the near surface winds (Smith et al., 2013).

Stationary katabatic jumps occur at the surface of the Antarctic ice sheet (Pettré and André, 1991); they could lead to the formation of terrestrial equivalents of the Martian large sedimentation waves. These terrestrial equivalents have not been discovered so far however, perhaps because the small dust content in the Antarctic ice relative to the Martian ice does not allow the development of significant albedo contrasts between megadune upwind and downwind sides, while such albedo contrasts have been argued to promote the growth of large sedimentation waves on Mars (Ivanov and Muhleman, 2000; Ng and Zuber, 2006).

4.4. Remaining questions

Major issues on the dynamics of Martian sedimentation waves and Antarctic megadunes remain to be resolved.

(1) While one wavelength only has been described so far for Antarctic megadunes, there are two wavelengths of sedimentation wave on the Martian North Polar Cap. The relation between these two wavelengths is unclear. Do they develop independently or do the large ones control the formation of the small ones, as was suggested by Howard (2000) and Smith et al. (2013)? Do the large ones result from the development of the small ones (Howard, 2000)? Does a terrestrial equivalent exist for the large ones?

(2) Accumulation on Antarctic megadunes fields is thought to be dominated by the deposition of wind-blown snow particles (Goodwin, 1990; Rémy and Frezzotti, 2006), when accumulation on the Martian North Polar Cap is generally attributed to direct condensation of atmospheric water vapor onto the ice cap surface (Ivanov and Muhleman, 2000; Ng and Zuber, 2006). The respective contributions of atmospheric precipitation and direct condensation thus remain to be fully evaluated both in Antarctica and on Mars.

(3) Seasonal variations in short-term accumulation and ablation rates on either side of sedimentation waves are still to be assessed on Earth and on Mars. In other words, do the asymmetry in long-term net accumulation/ablation rates across sedimentation waves and megadunes results from an asymmetry in seasonal accumulation rates, in seasonal sublimation rates, or both?

5. Conclusion

The Martian North Polar Cap and the Antarctic Ice Sheet interact with cold and dry atmospheres, have low accumulation rates and are subject to permanent and uniform katabatic wind regimes.

These environmental similarities lead to the development of analog ice/wind interaction features on their surfaces. These include sedimentation waves that are comparable in their surface morphology, texture, grain size, and internal stratigraphic architecture. Their shallow-dipping upwind sides, their tops and the intervening troughs are covered by young ice and occasional sastrugi fields, indicative of net accumulation. On the other hand, their steep-dipping downwind sides either expose exhumed layers of old ice or correspond to smooth surfaces of coarse-grained ice, indicative of net ablation or reduced net accumulation associated with sublimation and metamorphism. These surface characteristics and the internal stratigraphic architecture revealed by radar sounding are consistent with the interpretation that these sedimentation waves grow and migrate upwind in response to the development of periodic accumulation/ablation patterns controlled by katabatic winds.

In Antarctica, only one wavelength has been described so far for these sedimentation waves. By contrast, the Martian North Polar Cap displays two superimposed sets of sedimentation wave with differing wavelengths. The smaller waves, characterized by reduced net accumulation on their downwind sides, are probably Martian ice megadunes analogous to the Antarctic megadunes that have been described so far. On the other hand, a terrestrial equivalent remains to be discovered for the larger sedimentation waves, characterized by net ablation on their downwind sides.

This work provides a basis for the future development of a common model of ice/wind interaction at the surface of Martian and terrestrial glaciers. A clear understanding of these interactions is of primary importance for the climatic interpretation of ice records and for the assessment of processes and rates of mass and heat transfers in glaciers on Earth and on Mars.

Acknowledgements

This work benefited from financial supports from the Center National de la Recherche Scientifique (CNRS), Centre National d'Études Spatiales, Institut National des Sciences de l'Univers (INSU), Programme National de Planétologie (PNP), Agence Nationale de la Recherche (Project ANR-12-BS05-001 EXODUNES), ATLAB project from the European program RegPot and the Fundation for Polish Science project (FNP) TEAM/2011-7/9. C. Hery is supported by a Ph.D. research grant from the French government (Ministère de l'Enseignement Supérieur et de la Recherche). We thank S. Pochat, S. Douté and L. Perret for the constructive discussions. We are grateful to R. Dacic and an anonymous reviewer for their insightful comments on a preliminary version of the article.

References

- Albert, M., Shuman, C.A., Courville, Z., Bauer, R., Fahnestock, M., Scambos, T., 2004. Extreme firn metamorphism: impact of decades of vapor transport on near-surface firn at a low-accumulation glazed site on the East Antarctic plateau. *Ann. Glaciol.* 39 (1), 73–78. <http://dx.doi.org/10.3189/172756404781814041>.
- Andreotti, B., Fourrière, A., Ould-Kaddour, F., Murray, B., Claudin, P., 2009. Giant aeolian dune size determined by the average depth of the atmospheric boundary layer. *Nature* 457 (7233), 1120–1123. <http://dx.doi.org/10.1038/nature07787>.
- Anschütz, H., Eisen, O., Rack, W., Scheinert, M., 2006. Periodic surface features in coastal East Antarctica. *Geophys. Res. Lett.* 33 (22), 501. <http://dx.doi.org/10.1029/2006GL027871>.
- Appéré, T., Schmitt, B., Langevin, Y., Douté, S., Pommerol, A., Forget, F., Spiga, A., Gondet, B., Bibring, J.-P., 2011. Winter and spring evolution of northern seasonal deposits on Mars from OMEGA on Mars Express. *J. Geophys. Res., Planets* 116 (E15), E05001. <http://dx.doi.org/10.1029/2010JE003762>.
- Arcone, S.A., Jacobel, R., Hamilton, G., 2012. Unconformable stratigraphy in East Antarctica: Part I. Large firn cosets, recrystallized growth, and model evidence for intensified accumulation. *J. Glaciol.* 58 (208), 240–252. <http://dx.doi.org/10.3189/2012Jof11J044>.
- Bagnold, R.A., 1954. *The Physics of Blown Sand and Desert Dunes*. Dover Publications, 265 pp.
- Banks, M.E., Byrne, S., Galla, K., McEwen, A.S., Bray, V.J., Dundas, C.M., Fishbaugh, K.E., Herkenhoff, K.E., Murray, B.C., 2010. Crater population and resurfacing of the Martian north polar layered deposits. *J. Geophys. Res.* 115 (E8). <http://dx.doi.org/10.1029/2009JE003523>.
- Bibring, J.-P., Soufflot, A., Berthé, M., Langevin, Y., Gondet, B., Drossart, P., Bouyé, M., Combes, M., Puget, P., Semery, A., Bellucci, G., Formisano, V., Moroz, V., Kottsov, V., Bonello, G., Erard, S., Forni, O., Gendrin, A., Manaud, N., Poulet, F., Poulleau, G., Encrenaz, T., Fouchet, T., Melchiorri, R., Altieri, F., Ignatiev, N., Titov, D., Zasova, L., Coradini, A., Capaciovani, F., Cerroni, P., Fonti, S., Mangold, N., Pinet, P., Schmitt, B., Sotin, C., Hauber, E., Hoffman, H., Jaumann, R., Keller, U., Arvidson, R., Mustard, J., Forget, F., 2004. OMEGA: observatoire pour la minéralogie, l'eau, les glaces et l'activité. *ESA SP* 1240, 37.
- Black, H., Budd, W., 1964. Accumulation in the region of Wilkes, Wilkes Land, Antarctica. *J. Glaciol.* 37 (5), 3–15.
- Bourke, M.C., Lancaster, N., Fenton, L.K., Parteli, E.J.R., Zimbleman, J.R., Radebaugh, J., 2010. Extraterrestrial dunes: an introduction to the special issue on planetary dune systems. *Geomorphology* 121 (1–2), 1–14. <http://dx.doi.org/10.1016/j.geomorph.2010.04.007>.
- Brown, A.J., Calvin, W.M., 2012. Water ice grain size evolution of Martian North Polar residual layered deposits for late summer MY28 and 30 from CRISM/MARCI observations. In: *43rd Lunar and Planetary Science Conference*, Houston, vol. 115, p. 1742.
- Claudin, P., Andreotti, B., 2006. A scaling law for Aeolian dunes on Mars, Venus, Earth, and for subaqueous ripples. *Earth Planet. Sci. Lett.* 252 (1–2), 30–44. <http://dx.doi.org/10.1016/j.epsl.2006.09.004>.
- Courville, Z.R., Albert, M.R., Fahnestock, M.A., Cathles IV, L.M., Shuman, C.A., 2007. Impacts of an accumulation hiatus on the physical properties of firn at a low-accumulation polar site. *J. Geophys. Res., Earth Surf.* 112 (F2), F02030. <http://dx.doi.org/10.1029/2005JF000429>.
- Cutts, J.A., Blasius, K.R., Roberts, W.J., 1979. Evolution of Martian polar landscapes: interplay of long-term variation in perennial ice cover and dust storm intensity. *J. Geophys. Res.* 84 (B6), 2975–2994. <http://dx.doi.org/10.1029/J084iB06p02975>.
- Clark, R., Roush, T., 1984. Reflectance spectroscopy: quantitative analysis techniques for remote sensing applications. *J. Geophys. Res.* 89 (B7), 6329–6340. <http://dx.doi.org/10.1029/JB089iB07p06329>.
- Dacic, R., Mott, R., Horgan, H.J., Lehning, M., 2013. Observations, theory, and modeling of the differential accumulation of Antarctic megadunes. *J. Geophys. Res., Earth Surf.* 118 (4), 2343–2353. <http://dx.doi.org/10.1002/2013JF002844>.
- Das, I., Bell, R.E., Scambos, T.A., Wolovick, M., Creyts, T.T., Studinger, M., Frearson, N., Nicolas, J.P., Lenaerts, J.T.M., van den Broeke, M.R., 2013. Influence of persistent wind scour on the surface mass balance of Antarctica. *Nat. Geosci.* 6 (5), 367–371. <http://dx.doi.org/10.1038/ngeo1766>.
- Dumont, M., Brissaud, O., Picard, G., Schmitt, B., Gallet, J.-C., Arnaud, Y., 2010. High-accuracy measurements of snow bidirectional reflectance distribution function at visible and NIR wavelengths – comparison with modelling results. *Atmos. Chem. Phys.* 10 (5), 2507–2520. <http://dx.doi.org/10.5194/acp-10-2507-2010>.
- Fahnestock, M.A., Scambos, T.A., Shuman, C.A., Arthern, R.J., Winebrenner, D.P., Kwok, R., 2000. Snow megadune fields on the East Antarctic Plateau: extreme atmosphere–ice interaction. *Geophys. Res. Lett.* 27 (22), 3719–3722. <http://dx.doi.org/10.1029/1999GL011248>.
- Fishbaugh, K.E., Hvidberg, C.S., 2006. Martian north polar layered deposits stratigraphy: implications for accumulation rates and flow. *J. Geophys. Res.* 111, E06012. <http://dx.doi.org/10.1029/2005JE002571>.
- Forget, F., Pollak, J.B., 1996. Thermal infrared observations of the condensing Martian polar caps: CO₂ ice temperatures and radiative budget. *J. Geophys. Res., Planets* 101 (E7), 16865–16879. <http://dx.doi.org/10.1029/96JE01077>.
- Flood, R.D., 1988. A lee wave model for deep-sea mudwave activity. *Deep-Sea Res.* 35 (6), 973–983. <http://dx.doi.org/10.1029/2001JD000673>.
- Frezzotti, M., Gandolfi, S., Urbini, S., 2002a. Snow megadunes in Antarctica: sedimentary structure and genesis. *J. Geophys. Res.* 107 (D18), 4344. <http://dx.doi.org/10.1029/2001JD000673>.
- Frezzotti, M., Gandolfi, S., 2002b. Snow dunes and glazed surfaces in Antarctica: new field and remote-sensing data. *Ann. Glaciol.* 34 (1), 81–88. <http://dx.doi.org/10.3189/172756402781817851>.
- Fuji, Y., Kusunoki, K., 1982. The role of sublimation and condensation in the formation of ice sheet surface at Mizuho Station, Antarctica. *J. Geophys. Res., Oceans* 87 (C6), 4293–4300. <http://dx.doi.org/10.1029/JC087iC06p04293>.
- Gay, M., Fily, M., Genthon, C., Frezzotti, M., Oerter, H., Winther, J.G., 2002. Snow grain-size measurements in Antarctica. *J. Glaciol.* 48 (163), 527–535. <http://dx.doi.org/10.3189/172756502781831016>.
- Goodwin, I.D., 1990. Snow accumulation and surface topography in the katabatic zone of Eastern Wilkes Land, Antarctica. *Antarct. Sci.* 2 (3), 235–242.
- Grima, C., Kofman, W., Mouginit, J., Phillips, R.J., Hérique, A., Biccari, D., Seu, R., Cutigni, M., 2009. North polar deposits of Mars: extreme purity of the water ice. *Geophys. Res. Lett.* 36 (3). <http://dx.doi.org/10.1029/2008GL036326>.
- Haberle, R.M., Forget, F., Colaprete, A., Schaffer, J., Boynton, W.V., Kelly, N.J., Chamberlain, M.A., 2008. The effect of ground ice on the Martian seasonal CO₂ cycle. *Planet. Space Sci.* 56 (2), 251–255. <http://dx.doi.org/10.1016/j.pss.2007.08.006>.
- Herkenhoff, K.E., Plaut, J.J., 2000. Surface ages and resurfacing rates of the Polar Layered Deposits on Mars. *Icarus* 144 (2), 243–253. <http://dx.doi.org/10.1006/icar.1999.6287>.
- Howard, A.D., 1978. Origin of the stepped topography of the Martian poles. *Icarus* 34 (3), 581–599.

- Howard, A.D., Cutts, J.A., Blasius, K.R., 1982. Stratigraphic relationships within Martian polar cap deposits. *Icarus* 50 (2–3), 161–215. [http://dx.doi.org/10.1016/0019-1035\(82\)90125-7](http://dx.doi.org/10.1016/0019-1035(82)90125-7).
- Howard, A.D., 2000. The role of eolian processes in forming surface features of the Martian Polar Layered Deposits. *Icarus* 144 (2), 267–288. <http://dx.doi.org/10.1006/icar.1999.6305>.
- Ivanov, A.B., Muhleman, D.O., 2000. The role of sublimation for the formation of the Northern Ice Cap: results from the Mars Orbiter Laser Altimeter. *Icarus* 144 (2), 436–448. <http://dx.doi.org/10.1006/icar.1999.6304>.
- Jakosky, B.M., Farmer, C.B., 1982. The seasonal and global behavior of water vapor in the Mars atmosphere: complete global results of the Viking atmospheric water detector experiment. *J. Geophys. Res.* 87 (B4), 2999–3019. <http://dx.doi.org/10.1029/JB087iB04p02999>.
- Jaumann, R., Neukum, G., Behnke, T., Duxbury, T.C., Eichtenopf, K., Flohrer, J., Gasselt, S.V., Giese, B., Gwinner, K., Hauber, E., Hoffmann, H., Hoffmeister, A., Köhler, U., Matz, K.-D., McCord, T.B., Mertens, V., Oberst, J., Pischel, R., Reiss, D., Ress, E., Roatsch, T., Saiger, P., Scholten, F., Schwarz, G., Stephan, K., Wählisch, M., The HRSC Co-Investigator Team 1, 2007. The high-resolution stereo camera (HRSC) experiment on Mars Express: instrument aspects and experiment conduct from interplanetary cruise through the nominal mission. *Planet. Space Sci.* 55 (7), 928–952. <http://dx.doi.org/10.1016/j.pss.2006.12.003>.
- Kostic, S., Sequeiros, Octavio, Spinewine, B., Parker, G., 2010. Cyclic steps: a phenomenon of supercritical shallow flow from the high mountains to the bottom of the ocean. *J. Hydro-Environ. Res.* 3 (4), 167–172. <http://dx.doi.org/10.1016/j.jher.2009.10.002>.
- Langevin, Y., Poulet, F., Bibring, J.-P., Douté, S., Gondet, B., 2005. Summer evolution of the North Polar Cap of Mars as observed by OMEGA/Mars Express. *Science* 307, 1581–1584. <http://dx.doi.org/10.1126/science.1109438>.
- Laskar, J., Levrard, B., Mustard, J.F., 2002. Orbital forcing of the Martian polar layered deposits. *Nature* 419 (6905), 375–377. <http://dx.doi.org/10.1038/nature01066>.
- Lee, H.J., Syvitski, J.P.M., Parker, G., Orange, D., Locat, J., Hutton, E.W.H., Imran, J., 2002. Distinguishing sediment waves from slope failure deposits: field examples, including the ‘Humboldt slide’, and modelling results. *Mar. Geol.* 192 (1–2), 70–104. [http://dx.doi.org/10.1016/S0025-3227\(02\)00550-9](http://dx.doi.org/10.1016/S0025-3227(02)00550-9).
- Lenaerts, J.T.M., van den Broeke, M.R., van de Berg, E., van Meijgaard, E., Kuipers Munneke, P., 2012. A new high-resolution surface mass balance map of Antarctica (1979–2010) based on regional atmospheric climate modeling. *Geophys. Res. Lett.* 39, L04501. <http://dx.doi.org/10.1029/2011GL050713>.
- Lucey, P.G., Clark, R.N., 1985. Spectral properties of water ice and contaminants. In: *Ices in the Solar System*, vol. 156, pp. 155–168.
- Malin, M.C., Bell, J.F., Cantor, B.A., Caplinger, M.A., Calvin, W.M., Clancy, R.T., Edgett, K.S., Edwards, L., Haberle, R.M., James, P.B., Lee, S.W., Ravine, M.A., Thomas, P.C., Wolff, M.J., 2007. Context camera investigation on board the Mars Reconnaissance Orbiter. *J. Geophys. Res.* 112, E05S04. <http://dx.doi.org/10.1029/2006JE002808>.
- Massé, M., Bourgeois, O., Le Mouélic, S., Verpoorter, C., Le Deit, L., Bibring, J.-P., 2010. Martian polar and circum-polar sulfate-bearing deposits: sublimation tills derived from the North Polar Cap. *Icarus* 209 (2), 434–451. <http://dx.doi.org/10.1016/j.icarus.2010.04.017>.
- Massé, M., Bourgeois, O., Le Mouélic, S., Verpoorter, C., Spiga, A., Le Deit, L., 2012. Wide distribution and glacial origin of polar gypsum on Mars. *Earth Planet. Sci. Lett.* 317–318 (1–2), 44–55. <http://dx.doi.org/10.1016/j.epsl.2011.11.035>.
- Milkovich, S.M., Head III, J.W., Neukum, G., The HRSC Co-Investigator Team, 2008. Stratigraphic analysis of the northern polar layered deposits of Mars: implications for recent climate history. *Planet. Space Sci.* 56 (2), 266–288. <http://dx.doi.org/10.1016/j.pss.2007.08.004>.
- Ng, F.S.L., Zuber, M.T., 2006. Patterning instability on the Mars polar ice caps. *J. Geophys. Res.* 111 (E2). <http://dx.doi.org/10.1029/2005JE002533>.
- Nolin, A.W., 1998. Mapping the Martian polar ice caps: applications of terrestrial optical remote sensing methods. *J. Geophys. Res.* 103 (E11), 25851–25864. <http://dx.doi.org/10.1029/98JE02082>.
- Nolin, A.W., Dozier, J., 2000. A hyperspectral method for remotely sensing the grain size of snow. *Remote Sens. Environ.* 74 (2), 207–216. [http://dx.doi.org/10.1016/S0034-4257\(00\)00111-5](http://dx.doi.org/10.1016/S0034-4257(00)00111-5).
- Painter, T.H., Dozier, J., Roberts, D.A., Davis, R.E., Green, R.O., 2003. Retrieval of sub-pixel snow-covered area and grain size from imaging spectrometer data. *Remote Sens. Environ.* 85 (1), 64–77. [http://dx.doi.org/10.1016/S0034-4257\(02\)00187-6](http://dx.doi.org/10.1016/S0034-4257(02)00187-6).
- Pankine, A.A., Tamppari, L.K., Smith, M.D., 2010. MGS TES observation of water vapor above the seasonal and perennial ice caps during northern spring and summer. *Icarus* 210 (1), 58–71. <http://dx.doi.org/10.1016/j.icarus.2010.06.043>.
- Pathare, A.V., Paige, D.A., 2005. The effects of Martian orbital variations upon the sublimation and relaxation of north polar troughs and scarps. *Icarus* 174 (2), 419–443. <http://dx.doi.org/10.1016/j.icarus.2004.10.030>.
- Parish, T.R., Bromwich, D.H., 1991. Continental-scale simulation of the Antarctic katabatic wind regime. *J. Climate* 4 (2), 135–146. [http://dx.doi.org/10.1175/15200442\(1991\)004<0135:CSSOTA>2.0.CO;2](http://dx.doi.org/10.1175/15200442(1991)004<0135:CSSOTA>2.0.CO;2).
- Pettré, P., André, J.C., 1991. Surface-pressure change through Loewe’s phenomena and katabatic flow jumps: study of two cases in Adelie Land, Antarctica. *J. Atmos. Sci.* 48 (4), 557–571. [http://dx.doi.org/10.1175/1520-0469\(1991\)048<0557:SPCTLP>2.0.CO;2](http://dx.doi.org/10.1175/1520-0469(1991)048<0557:SPCTLP>2.0.CO;2).
- Putzig, N.E., Phillips, R.J., Campbell, B.A., Holt, J.W., Plaut, J.J., Carter, L.M., Egan, A.F., Bernardini, F., Safaeinili, A., Seu, R., 2009. Subsurface structure of Planum Boreum from Mars Reconnaissance Orbiter Shallow Radar soundings. *Icarus* 204 (2), 443–457. <http://dx.doi.org/10.1016/j.icarus.2009.07.034>.
- Rémy, F., Frezzotti, M., 2006. Antarctica ice sheet mass balance. *C. R. Géosci.* 338 (14–15), 1084–1097. <http://dx.doi.org/10.1016/j.crte.2006.05.009>.
- Rodriguez, J.A.P., Tanaka, K.L., Langevin, Y., Bourke, M., Kargel, J., Christensen, P., Sasaki, S., 2007. Recent Aeolian erosion and deposition in the North Polar Plateau of Mars. *Mars* 3, 29–41. <http://dx.doi.org/10.1555/mars.2007.0003>.
- Scambos, T., Haran, T., Fahnestock, M., Painter, T., Bohlander, J., 2007. MODIS-based Mosaic of Antarctica (MOA) data sets: continent-wide surface morphology and snow grain size. *Remote Sens. Environ.* 111 (2–3), 242–257. <http://dx.doi.org/10.1016/j.rse.2006.12.020>.
- Scambos, T.A., Frezzotti, M., Haran, T., Bohlander, J., Lenaerts, J.T.M., van den Broeke, M.R., Jezek, K., Long, D., Urbini, S., Farness, K., Neumann, T., Albert, M., Winther, J.-G., 2012. Extent of low-accumulation ‘wind glaze’ areas on the East Antarctic plateau: implications for continental ice mass balance. *J. Glaciol.* 58 (210), 633–647. <http://dx.doi.org/10.3189/2012JG11J232>.
- Seu, R., Phillips, R.J., Biccari, D., Orosei, R., Masdea, A., Picardi, G., Safaeinili, A., Campbell, B.A., Plaut, J.J., Marinangeli, L., Smeke, S.E., Nunes, D.C., 2007. SHARAD sounding radar on the Mars Reconnaissance Orbiter. *J. Geophys. Res.* 112 (E5), 157–166. <http://dx.doi.org/10.1029/2006JE002745>.
- Smith, D.E., Zuber, M.T., Frey, H.V., Garvin, J.B., Head, J.W., Muhleman, D.O., Pettengill, G.H., Phillips, R.J., Solomon, S.C., Zally, H.J., Banerdt, W.B., Duxbury, T.C., Golombek, M.P., Lemoine, F.G., Neumann, G.A., Rowlands, D.D., Aharonson, O., Ford, P.G., Ivanov, A.B., Johnson, C.L., McGovern, P.J., Abshire, J.B., Afzal, R.S., Sun, X., 2001. Mars Orbiter Laser Altimeter (MOLA): experiment summary after the first year of global mapping of Mars. *J. Geophys. Res.* 106 (E10), 23689–23722. <http://dx.doi.org/10.1029/2000JE001364>.
- Smith, I.B., Holt, J.W., 2010. Onset and migration of spiral troughs on Mars revealed by orbital radar. *Nature* 465 (7297), 450–453. <http://dx.doi.org/10.1038/nature09049>.
- Smith, I.B., Holt, J.W., Spiga, A., Howard, A.D., Parker, G., 2013. The spiral troughs of Mars as cyclic steps. *J. Geophys. Res., Planets* 118 (9), 1835–1857. <http://dx.doi.org/10.1002/jgre.20142>.
- Sori, M.M., Perron, J.T., Huybers, P., Aharonson, O., 2014. A procedure for testing the significance of orbital tuning of the Martian polar layered deposits. *Icarus* 235, 136–146. <http://dx.doi.org/10.1016/j.icarus.2014.03.009>.
- Spiga, A., 2011. Elements of comparison between Martian and terrestrial mesoscale meteorological phenomena: katabatic winds and boundary layer convection. *Planet. Space Sci.* 59 (10), 915–922. <http://dx.doi.org/10.1016/j.pss.2010.04.025>.
- Sqyres, S.W., 1979. The evolution of dust deposits in the Martian Polar Region. *Icarus* 40 (2), 244–261. [http://dx.doi.org/10.1016/0019-1035\(79\)90070-8](http://dx.doi.org/10.1016/0019-1035(79)90070-8).
- Taffin, C., Grasset, O., Le Menn, E., Bollengier, O., Giraud, M., Le Mouélic, S., 2012. Experimental study of water ice IR signature dependence with temperature and grain size. Application to Enceladus. *Planet. Space Sci.* 61 (1), 124–134. <http://dx.doi.org/10.1016/j.pss.2011.08.015>.
- Tanaka, K.L., Rodriguez, J.A.P., Skinner, J.A., Bourke, M.C., Fortezzo, C.M., Herkenhoff, K.E., Kolb, E.J., Okubo, C.H., 2008. North polar region of Mars: advances in stratigraphy, structure, and erosional modification. *Icarus* 196 (2), 318–358. <http://dx.doi.org/10.1016/j.icarus.2008.01.021>.
- Tomasi, C., Petkov, B.H., Benedetti, H., 2012. Annual cycles of pressure, temperature, absolute humidity and precipitable water from the radiosoundings performed at Dome C, Antarctica, over the 2005–2009 period. *Antarct. Sci.* 24 (6), 637–658. <http://dx.doi.org/10.1017/S0954102012000405>.
- Vincendon, M., Langevin, Y., Poulet, F., Bibring, J.-P., Gondet, B., 2007. Recovery of surface reflectance spectra and evaluation of the optical depth of aerosols in the near-IR using a Monte Carlo approach: application to the OMEGA observations of high-latitude regions of Mars. *J. Geophys. Res., Planets* 112 (E8), E08S13. <http://dx.doi.org/10.1029/2006JE002845>.
- Warren, S.G., 1982. Optical properties of snow. *Rev. Geophys. Space Phys.* 20 (1), 67–89. <http://dx.doi.org/10.1029/RG020i001p0067>.
- Whiteway, J.A., Konguem, L., Dickinson, C., Cook, C., Illnicki, M., Seabrook, J., Popvici, V., Duck, T.J., Davy, R., Taylor, P.A., Pathak, J., Fisher, D., Carswell, A.I., Daly, M., Hipkin, V., Zent, A.P., Hecht, M.H., Wood, S.E., Tamppari, L.K., Renno, N., Moores, J.E., Lemmon, M.T., Daerden, F., Smith, P.H., 2009. Mars water-ice clouds and precipitation. *Science* 325 (5936), 68–70. <http://dx.doi.org/10.1126/science.1172344>.
- Zuber, M., Lim, L., Zwally, H., 1998. The role of viscous deformation in the morphology of the Martian North Polar Cap. In: *First International Conference on Mars Polar Science*, pp. 45–46.